Catal Lett (2017) 147:1844–1850
DOI 10.1007/s10562-017-2094-5

Solvothermal Synthesis of *p*-type Cu_2ZnSnS_4-Based Nanocrystals and Photocatalytic Properties for Degradation of Methylene Blue

Hao Guan[1,2] · Honglie Shen[1] · Adil Raza[1]

Received: 24 March 2017 / Accepted: 24 May 2017 / Published online: 29 May 2017

Abstract The quaternary copper-based chalcogenide Cu_2ZnSnS_4 (CZTS), have recently arisen as a low-cost and environment-friendly material for photovoltaics and photocatalysis. In this paper, *p*-type kesterite Cu_2ZnSnS_4 (CZTS) nanocrystals were synthesized by solvothermal method. X-ray diffraction (XRD), Raman spectroscopy, Scanning electron microscopy (SEM) and UV–Vis spectroscopy were used to investigate the structural, morphological and photocatalytic properties of kesterite CZTS nanocrystals. The kesterite CZTS nanocrystals powder were used as a photocatalyst to investigate the degradation rate of methylene blue (MB) under visible-light irradiation. The results show the 62% degradation of methylene blue (MB) within 240 min under visible-light irradiation. Furthermore, Zn was partially doped with Fe, Mn, Co, and Ni. CZTS-based nanocrystals and results reveal that $Cu_2(Zn_{0.8}Me_{0.2})SnS_4$ (Me = Fe, Mn, Co, Ni) could degrade 92, 74, 84 and 89% of MB within 240 min, respectively, indicating promising potential as effective visible-light photocatalysts.

Graphical Abstract

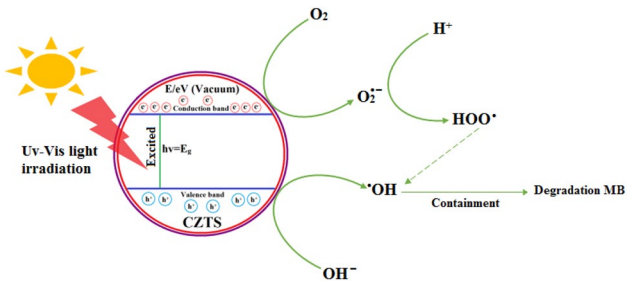

Keywords CZTS-based · Nanocrystals · Solvothermal · Visible-light photocatalytic properties

1 Introduction

Semiconductor materials with stable physical and chemical properties to photo-catalytic degradation of pollutants have gained substantial attention. Semiconductor photocatalysis is a progressive technology that initiates the holes on the valence band and electrons on the conduction band after band gap excitation, pollutants can be decomposed by photo-oxidization or photo-reduction reaction. For a photocatalytic reaction, an ideal semiconductor photocatalyst should be: (I) photo-active; (II) capable of utilizing visible and UV light; (III) chemically and biologically inert; (IV) photo-stable; (V) low-cost. As agreed by most studies, TiO_2 basically fulfills the whole criteria (I–V) and is one of the most recognized and widely used photocatalysts [1–3]. More recently, the *n*-type semiconductor photocatalysts have been researched in-depth, such as ZnO [4], CdS [5] and TiO_2 [6–8]. However, these *n*-type photocatalysts have wide

✉ Honglie Shen
hlshenktz@163.com

[1] College of Materials Science and Technology, Nanjing University of Aeronautics and Astronautics, 29 Yudao Street, Nanjing 210016, People's Republic of China

[2] School of Materials Engineering, Yancheng Institute of Technology, 9 Yinbing Street, Yancheng 224051, People's Republic of China

band gaps and can be used in UV illumination. As for *p*-type semiconductor photocatalysts, there is very few related literature.

The semiconductor TiO_2 is one of the best photocatalysts due to its many advantages such as high chemical stability, green, low-cost and high-power efficiency etc. However, a pure TiO_2 can absorb barely 3–5% of visible light in solar spectrum due to its wide bandgap ($E_g \geq 3.0$ eV), which greatly limits its application in visible-light photocatalysis. There are some drawbacks in the use of TiO_2 in powder form during photocatalytic processes, namely: (i) difficulty in fully separating it from aqueous solution, (ii) tendency to aggregate at high concentrations, and (iii) difficulty in recycling the material [1, 7]. Consequently, extensive research works have focused on discovering advance photo-sensitizer materials, which need to be highly efficient, offer a long functional lifetime, earth abundant and inexpensive has generated great interest in area of photocatalysis research.

In recent decades, quaternary copper-based chalcogenide Cu_2ZnSnS_4 (CZTS) has emerged as a most promising candidate for both economic and ecological thin film solar cells studies with elemental abundance, favorably matched band gap (1.1–1.5 eV) to solar spectrum, high optical absorption coefficient ($\geq 10^4$ cm^{-1}), relative abundance of the component elements with excellent photostability and low toxicity and various synthetic methods [9–11]. Maximizing material performance in a particular application frequently requires the simultaneous optimization of several functional properties. In the field of photocatalysis, the material needs to be able to absorb the major part of the solar spectra, to adsorb the reactants and generally to efficiently exchange charge with them. The quaternary chalcogenide semiconductors such as Cu_2ZnSnS_4, Cu_2FeSnS_4, Cu_2MnSnS_4, Cu_2CoSnS_4 and Cu_2NiSnS_4 have similar structures. The optical band gap can be tuned by Fe, Mn, Co, Ni substituting for Zn in visible-light range, and we believe that the photocatalytic properties of CZTS nanocrystals can be improved by doping. As far as we all know, no report have been found to study photocatalytic properties of doped CZTS nanocrystals.

Herein, flower-like CZTS nanocrystals were synthesized using the solvothermal method. Structural, morphological properties were investigated by different characterizing techniques such as X-Ray diffraction (XRD), Raman spectroscopy and Scanning electron spectroscopy (SEM). The photocatalytic properties of *p*-type Cu_2ZnSnS_4-based nanocrystals were evaluated by degrading the methylene blue (MB) dye under visible light irradiation. The photocatalytic properties of doped $Cu_2(Zn_{0.8}Me_{0.2})SnS_4$ (Me = Fe, Mn, Co, Ni) were also investigated for MB dye under the same conditions.

2 Experimental Details

2.1 Materials

Cupric chloride dihydrate ($CuCl_2{\cdot}2H_2O$), zinc acetate dihydrate [$Zn(CH_3COO)_2{\cdot}2H_2O$], Iron(III) nitrate nonahydrate [$Fe(NO_3)_3{\cdot}9H_2O$], Cobalt(II) acetate tetrahydrate [$Co(CH_3COO)_2{\cdot}4H_2O$], Manganese(II) acetate tetrahydrate [$Mn(CH_3COO)_2{\cdot}4H_2O$], Nickel(II) acetate tetrahydrate [$Ni(CH_3COO)_2{\cdot}4H_2O$], Tin(II) chloride dehydrate ($SnCl_2{\cdot}2H_2O$) and Thiourea (H_2NCSNH_2) are of analytical grade, used without any further purification.

2.2 Preparation of CZTS Nanocrystals

In this experiment, $CuCl_2{\cdot}2H_2O$ (2M), $Zn(CH_3COO)_2{\cdot}2H_2O$ (1M), $SnCl_2{\cdot}2H_2O$ (1 M) and H_2NCSNH_2 (4M) were added in 40 ml ethylene glycol to dissolve under sustained stirring at 45 °C for 40 min until have a clear yellow colloidal suspension. Furthermore, the obtained clear colloidal suspension was placed in a 50 ml Teflon autoclave. Thereafter, tightly closed autoclave was heated at 200 °C for 24 h and followed by, left to cool at ambient conditions. The precipitates were collected by centrifugation, washed with ethanol and deionized water several times and then dried under vacuum at 80 °C for 3 h. Furthermore, Doped $Cu_2(Zn, Me)SnS_4$ (Me = Fe, Mn, Co, Ni) nanocrystals were also synthesized by following the same procedure. The as-obtained products could be achieved reproducibly owing to simple and mild reaction.

2.3 Characterization

The phase and crystallographic information of CZTS nanocrystals were obtained from the X-ray diffraction patterns (PANalytical X'Pert PRO diffractometer with Cu $K\alpha$ radiation, $\lambda = 0.15406$ nm,) and JY-T64000 Raman spectroscopy. Surface morphologies of the as-synthesized samples were characterized using LEO-1530VP scanning electron microscope (SEM). UV–Vis spectrophotometer (UV-2450, Shimadzu) was used to study the photocatalytic degradation of MB dye.

2.4 Photocatalytic Reaction

The photocatalytic reaction of CZTS-based nanocrystals was determined by degradation of methylene blue (MB) dye in an aqueous solution under exposure of UV–Vis light. Initially, a 0.05 g of as-prepared CZTS-based nanocrystals powder were added to 50 ml of MB solution with the concentration of 10^{-5} mol/l. The solutions were stirred under no light irradiation for 30 min to achieve the adsorption–desorption equilibrium between the catalyst and MB

dye solution before visible light irradiation. Furthermore, the solutions were exposed to visible light under continuous stirring. At given time intervals, a small amount of as-obtained solution were measured as samples after removing CZTS-based nanocrystals.

3 Results and Discussion

X-ray powder diffraction (XRD) pattern and Raman spectrum of as-synthesized CZTS nanocrystals are shown in Fig. 1a, b. It can be seen from Fig. 1a, all the diffraction peaks are well indexed with the kesterite structure of CZTS (JCPDS No. 26-0575). The main diffraction peaks at $2\theta = 28.7°$, 32.8°, 47.2° and 56.4° can be attributed to the (112), (200), (220) and (312) plans of CZTS, respectively. Figure 1a shows no any other binary/tertiary byproducts from other crystalline forms. The calculated lattice parameters are $a = b = 5.437$ Å and $c = 10.805$ Å, which are in good agreement with standard CZTS powder data. Moreover, the average grain size can be calculated by Debye–Scherrer formula. The average grain size is found to be about 4.69 nm. The sharp peaks in XRD pattern indicate the obtained CZTS nanocrystals have higher nanocrystallinity. It means higher nanocrystallinity leads to an addition in the surface areas, thus enhance the adsorption of reactants and subsequently higher the photo-reactivity. The CZTS structure needs to distinguish further due to its similarity to that of Cu_2SnS_3 and ZnS. In order to further ensure the structural homogeneity, Raman measurement was taken. A strong peak at 337 cm^{-1} corresponding to a kesterite CZTS can be seen from Fig. 1b. Which is in good agreement with that of CZTS nanocrystals reported in the literature [12]. No additional peaks for other phases, such as ZnS (274 and 351 cm^{-1}) and Cu_2SnS_3 (290, 318, and 348 cm^{-1}) are seen, indicating the single phase of the CZTS nanocrystals. The results above show that the preparation conditions are proper.

Figure 2a shows the indexed XRD patterns of solvothermal synthesized $Cu_2(Zn_{0.8}Me_{0.2})SnS_4$ (Me = Fe, Mn, Co, Ni). This patterns are also well-matched with the pure phase kesterite CZTS. It can be seen that kesterite CZTS structures are not be changed by partially substituting Zn with Fe, Mn, Co, Ni. However, the crystallinity of doped $Cu_2(Zn_{0.8}Me_{0.2})SnS_4$ (Me = Fe, Mn, Co, Ni) samples is less compared to CZTS nanocrystals. No secondary phase except for the (112), (220) and (312) plans of CZTS, are observed, indicating that synthesized $Cu_2(Zn_{0.8}Me_{0.2})SnS_4$ (Me = Fe, Mn, Co, Ni) samples are highly phases-pure. In addition, the Raman spectra of $Cu_2(Zn_{0.8}Me_{0.2})SnS_4$ (Me = Fe, Mn, Co, Ni) nanocrystals in Fig. 2b exhibit some major peaks (between 330 and 338 cm^{-1}) with broadness, which can be assigned to the A_1 mode of kesterite CZTS structure [13]. The significant changes in the Raman peak position with partially Fe, Mn, Co, Ni replacing Zn are not observed, indicating CZTS-based structural homogeneity, which is in accordance with XRD analysis.

The morphological and microstructural features of the as-obtained nanostructure were further investigated by using SEM. The different magnification SEM images of the CZTS nanocrystals are shown in Fig. 3a, b. The SEM images reveal that the CZTS as a representative hybrid material indicates that the as-obtained CZTS sample is composed of self-assembly flower-like structure with the petals thickness of about 60 nm (Fig. 3b). The definition of the flower-like CZTS structure comes from the geometrical similarity to flowers. The flower-like structure has a large surface area, aspect ratio whose internal parts

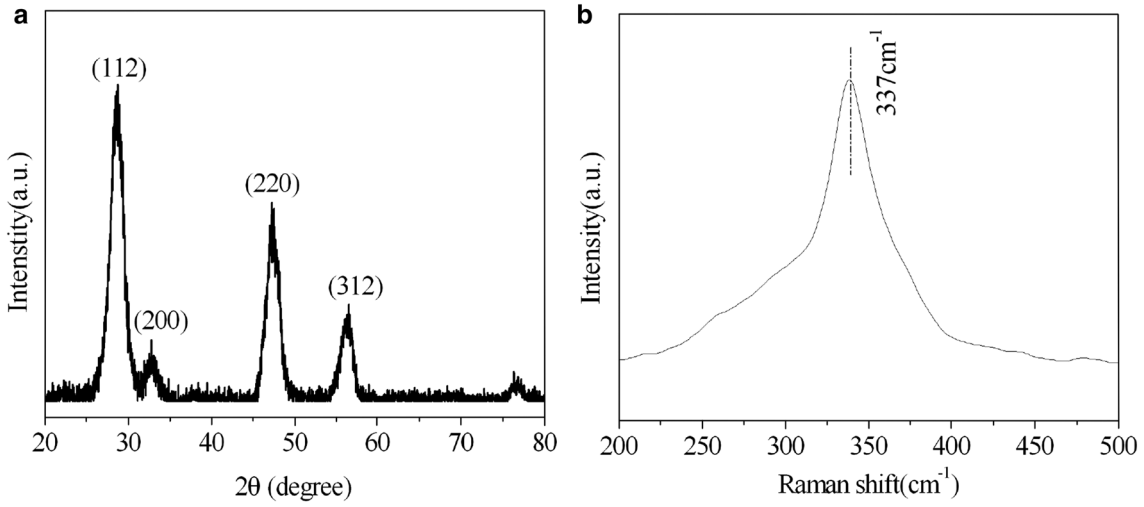

Fig. 1 **a** XRD patterns and **b** Raman spectrum of as-synthesized CZTS nanocrystals

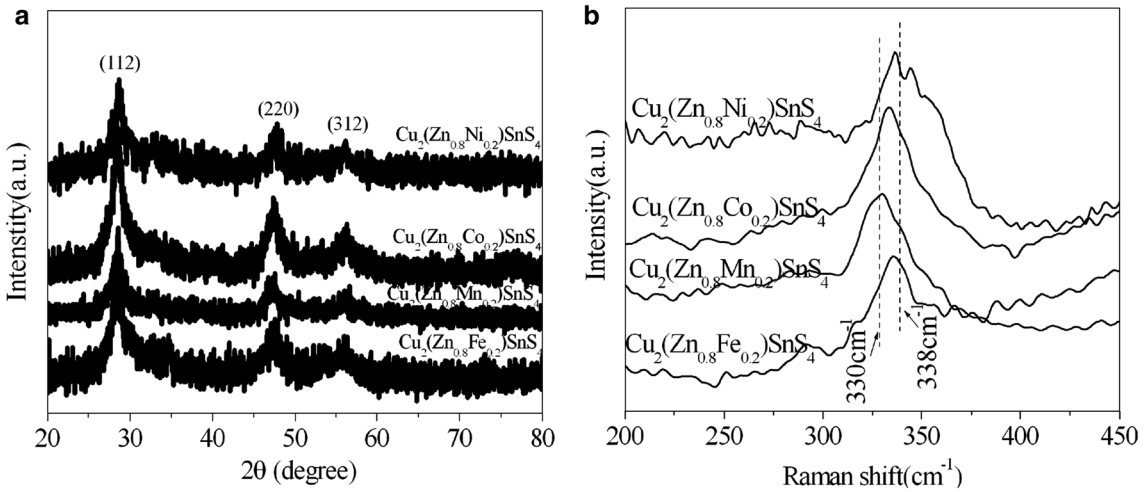

Fig. 2 **a** XRD patterns and **b** Raman spectra of as-synthesized partially substituted $Cu_2(Zn_{0.8}Me_{0.2})SnS_4$ (Me = Fe, Mn, Co, Ni) nanocrystals

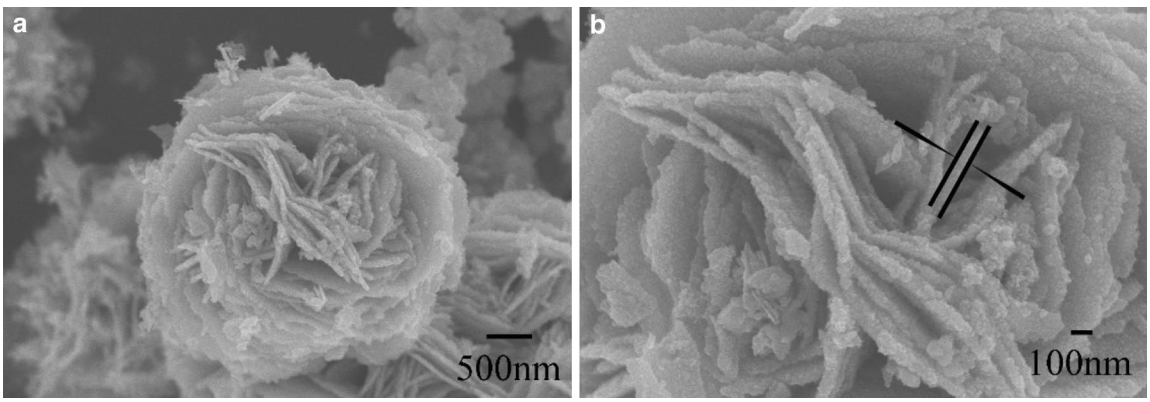

Fig. 3 SEM images of the flower-like CZTS structure with low (**a**) and high (**b**) magnifications

may not be fully utilized, which is helpful to improve the photocatalytic properties. The growth process of the self-assembly CZTS flower-like nanocrystals can be explained as follows: CZTS nanoparticles form through homogeneous nucleation and growth process followed by the formation of CZTS nanosheets owing to oriented aggregation. These building CZTS nanosheets further attach to flower-like particles through self-assembly process.

The SEM images of $Cu_2(Zn_{0.8}Me_{0.2})SnS_4$ (Me = Fe, Mn, Co, Ni) are shown in Fig. 4. It can be seen that all $Cu_2(Zn_{0.8}Me_{0.2})SnS_4$ (Me = Fe, Mn, Co, Ni) samples exhibit flower-like nanocrystals. Compared with pure CZTS nanocrystals, The thickness of the petals of $Cu_2(Zn_{0.8}Me_{0.2})SnS_4$ (Me = Fe, Mn, Co, Ni) crystals enhances due to grain growth being caused by the increasing of lattice energy. Meanwhile, we also can see that the surface of the petals of $Cu_2(Zn_{0.8}Me_{0.2})$ SnS_4(Me = Fe, Mn, Co, Ni) are rougher than that of CZTS nanocrystals, which help photocatalysis degradation.

Optical absorption characteristic is an important property of photocatalyst. UV–Vis absorption spectroscopy was used to investigate photocatalytic properties of the CZTS nanocrystals. It is well-accepted that the creation of e^-/h^+ pairs is the foremost reason of the photocatalytic reaction. The as-synthesized *p*-type CZTS semiconductor nanocrystals have holes as main carriers for the oxidation resistance. The band gap radiation can result in the redox reactions with adsorbed species over the surface of CZTS catalysts. It is believed that the photo-catalytic degradation of a dye takes place in the following manners: when UV–Vis radiation exposed over a catalyst, generation of electron–hole take place.

$$\mathrm{CZTS} + h\nu \rightarrow \mathrm{CZTS} + \mathrm{h}^+ + \mathrm{e}^- \quad (1)$$

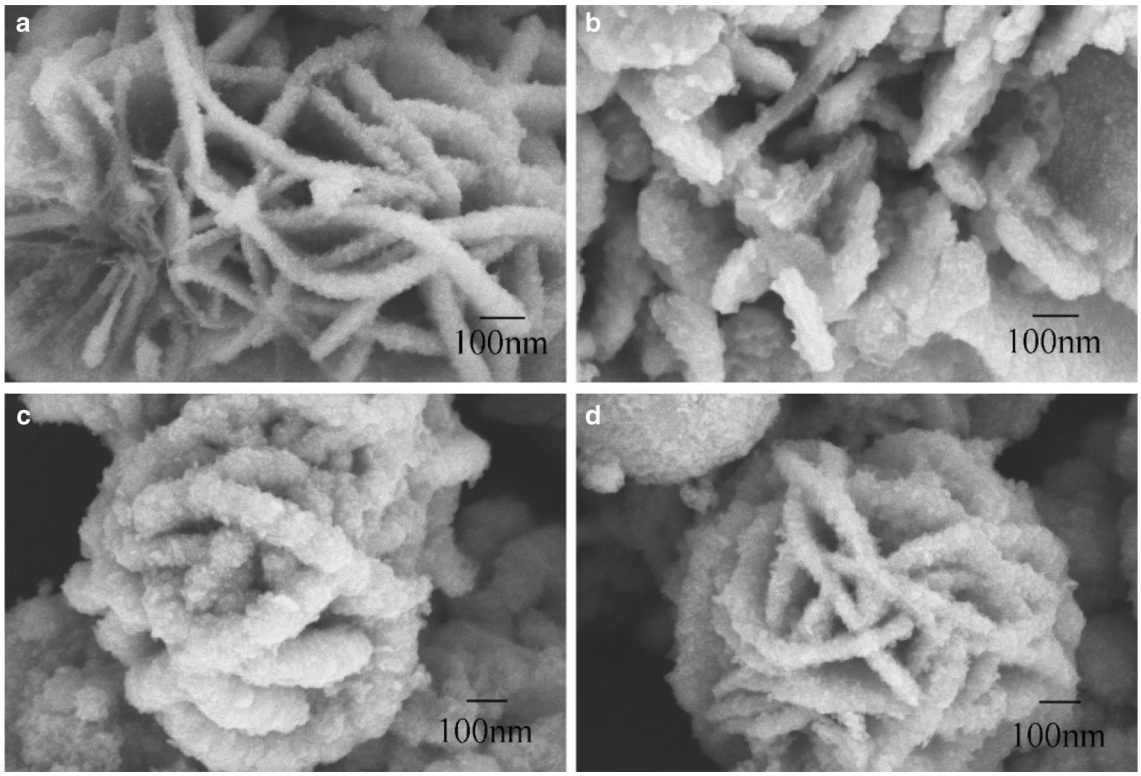

Fig. 4 SEM images of $Cu_2(Zn_{0.8}Me_{0.2})SnS_4$ (Me = Fe, Mn, Co, Ni) nanocrystals. **a** $Cu_2(Zn_{0.8}Fe_{0.2})SnS_4$, **b** $Cu_2(Zn_{0.8}Mn_{0.2})SnS_4$, **c** $Cu_2(Zn_{0.8}Co_{0.2})SnS_4$, **d** $Cu_2(Zn_{0.8}Ni_{0.2})SnS_4$

Together these entities migrate on the surface of CZTS catalyst, where a redox reaction takes place with other species which presents on the CZTS catalyst surface. In many circumstances, h^+ reacts with H_2O easily, which bounds on the CZTS catalyst surface and creates hydroxyl radicals, however, e^- reacts with O_2 and creates radicals. These electron and hole do not combine together.

$$H_2O + h^+ \rightarrow {}^{\bullet}OH + H^+ \quad (2)$$

$$O_2 + e^- \rightarrow {}^{\bullet}O_2^- \quad (3)$$

These produced $^{\bullet}$OH and radicals react with the MB dye to create additional species and consequently, responsible for the discoloration of MB dye.

$$^{\bullet}O_2^- + H^+ \rightarrow HOO^{\bullet} \quad (4)$$

$$H_2O_2 \rightarrow 2{}^{\bullet}OH \quad (5)$$

$$^{\bullet}OH + MB \rightarrow MB_{ox} \quad (6)$$

$$MB + e^- \rightarrow \text{intermediates} \rightarrow H_2O + CO_2 \quad (7)$$

A possible schematic mechanism is shown in Fig. 5. It should be noted that if both water and dissolved oxygen molecules are present then all above-mentioned steps in photocatalysis are possible. Highly reactive hydroxyl radicals ($^{\bullet}$OH) might not be created in the absence of water molecules, which prevent the photo-degradation of organic molecules in liquid phase [14]. The evaluation of the absorption spectra during the photodegradation of MB is shown in Fig. 6. The absorption spectra display the absorption at 662 ± 3 nm, however, It can be seen from Fig. 6a that the strength of the absorption peak decreases with increasing in exposure time, indicating CZTS nanocrystals have the ability for visible light photocatalytic decomposition of MB. It can be seen from Fig. 6b that the absorption equilibrium for the MB on the surface of flower-like CZTS nanocrystals is established for 30 min in the dark. Additionally, the curves in Fig. 6b show the degradation rates (c/c_0) of the Methylene Blue (MB) dye with and without CZTS nanocrystals under visible-light irradiation. It can be seen that in the presence of CZTS nanocrystals a 62% of the dye were decomposed in 240 min under exposure of visible light, while the photocatalytic degradation rate of MB without CZTS nanocrystals was about 3%.

The MB degradation rates (c/c_0) under visible-light for $Cu_2(Zn_{0.8}Me_{0.2})SnS_4$ (Me = Fe, Mn, Co, Ni) nanocrystals are shown in Fig. 7. After 240 min of visible-light irradiation, about 92, 74, 84 and 89% of MB were decomposed by $Cu_2(Zn_{0.8}Fe_{0.2})SnS_4$, $Cu_2(Zn_{0.8}Mn_{0.2})SnS_4$, $Cu_2(Zn_{0.8}Co_{0.2})SnS_4$ and $Cu_2(Zn_{0.8}Ni_{0.2})SnS_4$ nanocrystals, respectively.

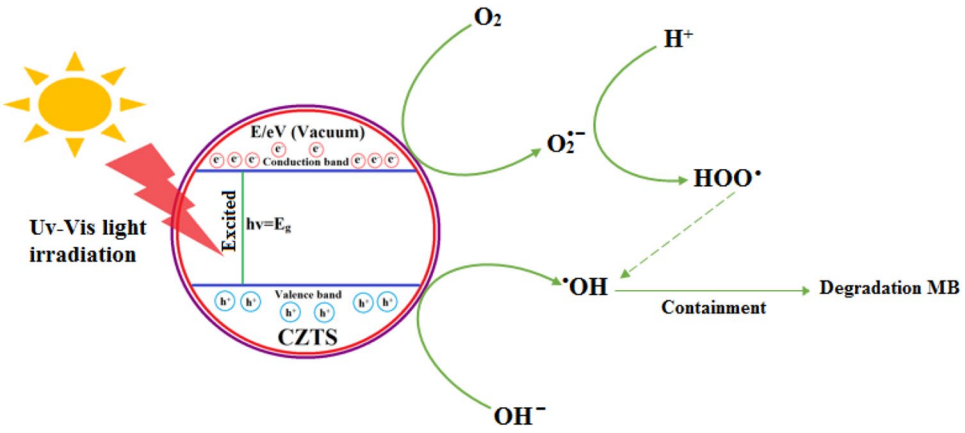

Fig. 5 Illustration of photocatalytic redox reaction occurring via photocatalysis to produce •OH to react with MB dye

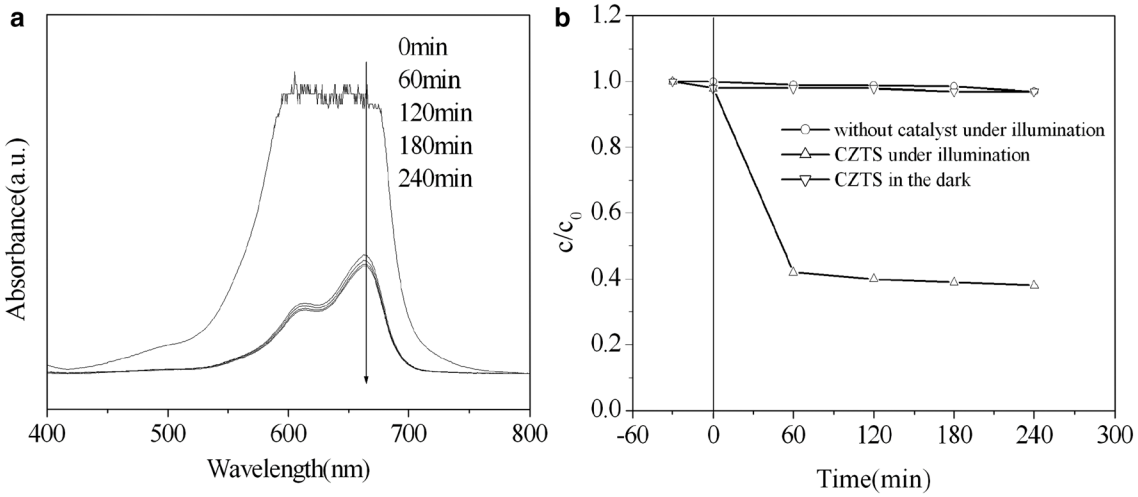

Fig. 6 **a** Absorption spectra of MB in the presence of CZTS nanocrystals under visible-light irradiation. **b** Photodegradation rate of MB as a function of different time with and without the addition of CZTS nanocrystals under illumination and with the addition of CZTS nanocrystals in the dark

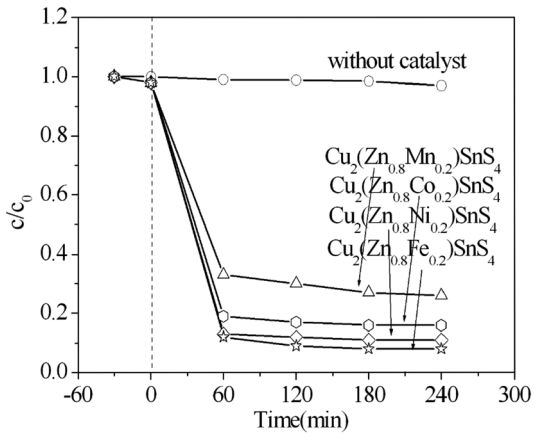

Fig. 7 The degradation rates of MB as a function of different time with and without of $Cu_2(Zn_{0.8}Me_{0.2})SnS_4$ (Me = Fe, Mn, Co, Ni) nanocrystals under visible-light

As we all know, the optical characteristic is a crucial property of photocatalyst [1]. It can be seen from Fig. 8 that the band gaps of doped CZTS nanocrystals are lower than that of CZTS nanocrystal, which can enhance the MB degradation rates by expanding visible light response. Meanwhile, The MB degradation rates of doped CZTS nanocrystals decrease with decreasing band gaps of the ones. As $Cu_2(Zn_{0.8}Fe_{0.2})SnS_4$ nanocrystal by small amounts of Fe^{3+} replacing Zn^{2+} increases concentration of electrons in the conduction band, the surface barrier becomes higher and the space charge region narrower [15]. The electron–hole pairs photogenerated with in this region are effectively seperated before the recombination [16]. It can improve photocatalytic activity. For $Cu_2(Zn_{0.8}Mn_{0.2})SnS_4$ nanocrystal, the low photocatalytic degradation rate of MB is also influenced by lattice distortion due to different ionic radius

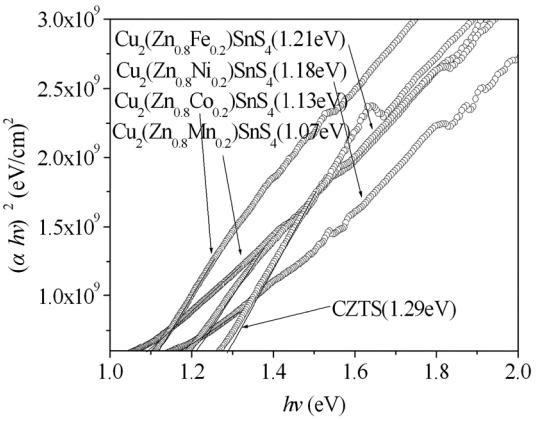

Fig. 8 Optical bandgap estimations of CZTS and Cu2(Zn0.8Me0.2) SnS4 (Me = Fe, Mn, Co, Ni) nanocrystals

[17]. For similar ionic radius of Zn^{2+} (0.074 nm), Co^{2+} (0.074 nm) and Ni^{2+} (0.072 nm), the photocatalytic degradation rate of MB for $Cu_2(Zn_{0.8}Co_{0.2})SnS_4$ is lower than that for $Cu_2(Zn_{0.8}Ni_{0.2})SnS_4$ due to a reduction in the surface areas being caused by too large grain size [1]. It is in accordance with XRD and SEM images.

4 Conclusions

In current research, we have successfully synthesized CZTS and $Cu_2(Zn_{0.8}Me_{0.2})SnS_4$ (Me = Fe, Mn, Co, Ni) nanocrystals by a solvothermal method. The as-obtained CZTS-based nanocrystals were characterized by XRD, SEM, Raman spectroscopy and UV–Vis spectroscopy. XRD results reveal that CZTS nanocrystals are single kesterite crystalline in natures, whereas $Cu_2(Zn_{0.8}Me_{0.2})SnS_4$ (Me = Fe, Mn, Co, Ni) nanocrystals are polycrystalline in nature. Surface morphology reveals that the CZTS nanocrystals were composed of flower-like particles, which could degrade about 62% of MB within 240 min under visible-light irradiation. The photocatalytic degradation rates of MB within 240 min for $Cu_2(Zn_{0.8}Fe_{0.2})SnS_4$, $Cu_2(Zn_{0.8}Mn_{0.2})SnS_4$, $Cu_2(Zn_{0.8}Co_{0.2})SnS_4$ and $Cu_2(Zn_{0.8}Ni_{0.2})SnS_4$ are about 92, 74, 84 and 89%, respectively, showing that CZTS is indeed a promising photocatalyst worthy of further study and providing an opportunity to solve pollutant problem in waste water.

Acknowledgements This research is financial supported by National Science Foundation of China (61176062), Project of Jiangsu Industry-Academia-Research (BY2015057-19), Funding of Jiangsu Innovation Program for Graduate Education (CXLX12_0146), the research fund of Jiangsu Province Cultivation base for State Key Laboratory of Photovoltaic Science and Technology (SKLPSTKF201506) and the Fundamental Research Funds for the Central Universities.

References

1. Hou X, Li Y, Yan J, Wang C (2014) Mater Res Bull 60:628
2. Ha E, Liu W, Wang LY, Man HW, Hu LS, Tsang SCE, Chan CTL, Kwok WM, Lee LYS, Wong KY (2017) Sci Rep 7:39411
3. Yu XL, An XQ, Aziz G, Ibáñez M, Arbiol J, Zhang YH, Cabot A (2015) J Phys Chem C 119:21882
4. Tripathy N, Ahmad R, Kuk H, Hahn YB, Khang G (2016) Ceram Int 42:9519
5. Li CM, He Y, Tang Q, Wang KT, Cui XM (2016) Mater Chem Phys 178:204
6. Liu X, Liu ZQ, Zheng J, Yan X, Li DD, Chen S, Chu W (2011) J Alloy Compd 509:9970
7. Martins AC, Cazetta A L, Pezoti O, Souza JRB, Zhang T, Pilau EJ, Asefa T, Almeida VC (2017) Ceram Int 43:4411
8. Anwar DI, Mulyadi D (2015) Procedia Chem 17:49
9. Mali SS, Patil PS, Hong CK (2014) ACS Appl Mater Interface 6:1688
10. Zhong J, Xia Z, Zhang C, Li B, Liu XS, Cheng YB, Tang J (2014) Chem Mater 26:3573
11. Wang W, Shen HL, He XC (2013) Mater Res Bull 48:3140
12. Rui TJM, Lee YH, Pedireddy S, Wong LH (2014) J Am Chem Soc 136:6684
13. Chen LL, Deng HM, Cui JY, Tao JH, Zhou WL, Cao HY, Sun L, Yang PX, Chu JH (2015) J Alloy Compd 627:388
14. Raza A, Azam A, Saeed MS, Ahsan M, Qayyum F, Yaseen M (2016) Dig J Nanomater Bios 11:1289
15. Kiriakidou F, Kondarides DI, Verykios XE (1999) Catal Today 54:119
16. Karakitsou K E, Verykios X E (1993) J Phys Chem 97:1184
17. Yue L H, Shui M, Xu Z D (1999) Acta Chim Sinica 57:1219